

Geophysical Research Letters

RESEARCH LETTER

10.1029/2021GL093277

Key Points:

- First results from the Scintillation Observations and Response of The Ionosphere to Electrodynamics (SORTIE) CubeSat show a large low-latitude ionospheric wavenumber-4 (WN4) structure observed concurrently by Ionospheric Connection Explorer (ICON) and Sounding of the Atmosphere using Broad band Emission Radiometry
- Spectral analyses of SORTIE Ion Velocity Meter (IVM), ICON IVM, and model output demonstrate that the diurnal eastward-propagating tide with zonal wavenumber 3 tide is responsible for this strong ionosphere-thermosphere (IT) WN4 coupling
- SORTIE and ICON IVM provide insights into tropical tropospheric influences on the IT by measuring poorly sampled altitudes simultaneously

Correspondence to:

F. Gasperini,
fgasperini@astraspace.net

Citation:

Gasperini, F., Azeem, I., Crowley, G., Perdue, M., Depew, M., Immel, T., et al. (2021). Dynamical coupling between the low-latitude lower thermosphere and ionosphere via the nonmigrating diurnal tide as revealed by concurrent satellite observations and numerical modeling. *Geophysical Research Letters*, 48, e2021GL093277. <https://doi.org/10.1029/2021GL093277>

Received 25 MAR 2021

Accepted 28 JUN 2021

Dynamical Coupling Between the Low-Latitude Lower Thermosphere and Ionosphere via the Nonmigrating Diurnal Tide as Revealed by Concurrent Satellite Observations and Numerical Modeling

Federico Gasperini¹ , Irfan Azeem¹ , Geoff Crowley¹ , Michael Perdue² , Matthew Depew², Thomas Immel³, Erik Stromberg¹, Chad Fish¹, Crystal Frazier¹, Adam Reynolds¹ , Anthony Swenson¹, Ted Tash¹, Russell Gleason¹, Ryan Blay¹ , Jordan Maxwell¹, Keith Underwood¹, Christian Frazier¹, and Scott Jensen¹

¹Atmospheric and Space Technology Research Associates, Louisville, CO, USA, ²William B. Hanson Center for Space Sciences, Physics Department, University of Texas at Dallas, Richardson, TX, USA, ³Space Sciences Laboratory, University of California, Berkeley, CA, USA

Abstract The diurnal eastward-propagating tide with zonal wavenumber 3 (DE3) is an important tidal component due to its ability to effectively couple the ionosphere-thermosphere with the tropical troposphere. In this work, we present the first results of a prominent zonal wavenumber-4 (WN4) structure in the low-latitude ionosphere observed by the Scintillation Observations and Response of The Ionosphere to Electrodynamics (SORTIE) CubeSat mission during May 27–June 5, 2020. Least squares analyses of concurrent in situ ion number density measurements from the SORTIE and the Ionospheric Connection Explorer satellites near 420 and 590 km show this pronounced WN4 to be driven by DE3. Thermosphere Ionosphere Mesosphere Energetics Dynamics Sounding of the Atmosphere using Broad band Emission Radiometry temperatures and Specified-Dynamics Whole Atmosphere Community Climate Model with thermosphere and ionosphere eXtension output demonstrate that the ionospheric WN4 structure is driven by DE3 propagating from the lower thermosphere.

Plain Language Summary The extent to which terrestrial weather (below ~30 km) can influence the ionosphere and thermosphere (IT) is a fascinating discovery of the last two decades or so. The IT is known to vary significantly from day to day, and this day-to-day weather is largely driven by processes originating in the lower atmosphere, especially during periods of quiet solar activity. Accurate forecasting of the IT variability thus depends on the ability to forecast the component that originates in the lower atmosphere. Ionospheric variability translates to uncertainty in navigation and communications systems, while thermospheric variability translates to uncertainty in orbital and reentry predictions. In this work, we present the first results from the Scintillation Observations and Response of The Ionosphere to Electrodynamics (SORTIE) CubeSat showing a large amplitude structure with four longitudinal peaks in the ionosphere associated with the well-known diurnal eastward-propagating tide with zonal wavenumber 3 originating in the tropical troposphere. Our analyses presented in this paper use concurrent SORTIE, Ionospheric Connection Explorer (ICON), and Thermosphere Ionosphere Mesosphere Energetics Dynamics satellite observations during May 27–June 5, 2020 and a whole atmosphere model to interpret SORTIE measurements. Our results suggest SORTIE and ICON to be excellent and complementary observational platforms for studying the influence of terrestrial weather on IT variability.

1. Introduction

The lower atmosphere drives variability in the ionosphere-thermosphere (IT) system through the vertical propagation of waves, including tides, planetary waves, and Kelvin waves. These waves are periodic in time and longitude due to the rotation of the Earth, and interact with the lower IT region to modulate electric fields that map to higher altitudes and redistribute plasma in the 200–1,000 km region. Due to the geometry of magnetic field lines near the equator, much of this variability occurs at low latitudes and is driven by waves that are excited by deep convective processes in the tropical troposphere and that propagate upwards

into the IT system. Tropical troposphere variability is essentially mapped to the IT system through a variety of neutral-plasma coupling processes, and over a range of spatial and temporal scales. One important class of global-scale atmospheric waves characterized by periods that are harmonics of a solar day are thermal tides. These atmospheric tides can be generated in different altitudinal regions due to tropospheric latent heating, absorption of tropospheric infrared radiation by water vapor, absorption of solar ultraviolet radiation by stratospheric ozone, thermosphere molecular oxygen absorption of extreme ultraviolet radiation, and wave-wave interactions (e.g., Chapman & Lindzen, 1970; Hagan & Forbes, 2002; Hagan et al., 2007; H.-L. Liu, 2016). The main pathways responsible for the modulation of the ionosphere by tides are direct propagation of atmospheric tides into the ionosphere and thermosphere (e.g., Hagan et al., 2007; Oberheide et al., 2009) and indirect coupling via the ionosphere E-region dynamo (e.g., Jin et al., 2008; Ren et al., 2010; Wan et al., 2008, 2010, 2012).

Several studies investigated the importance of IT variability driven by lower-atmosphere wave sources. Initial work (e.g., Fang et al., 2009; Hagan et al., 2007; Jin et al., 2008; Wan et al., 2010) focused on verifying Sagawa et al.'s (2005) and Immel et al.'s (2006) suggestion that the wavenumber-4 (hereafter, WN4) structure seen in satellite-borne Sun-synchronous F-region ionospheric data was due to the modulation of dynamo electric fields by nonmigrating tides propagating from below, and in particular due to the diurnal eastward-propagating tide with zonal wavenumber 3 ($s = -3$, i.e., DE3). DE3 originates in the tropical troposphere by latent heat release in deep convective clouds (e.g., Hagan, 1996; Hagan & Forbes, 2002; Lieberman et al., 2007), and its first equatorially symmetric Hough mode is the largest component in the lower thermosphere (Oberheide et al., 2009; Truskowski et al., 2014), capable of propagating well into the middle thermosphere (Gasperini et al., 2015, 2018; Gasperini, Forbes, & Hagan, 2017; Oberheide et al., 2011) due to its longer vertical wavelength. When viewed at quasi-fixed local time (LT) from slowly precessing satellites, this feature manifests as a 4-peak longitude structure. Subsequent studies examined the LT and seasonal variations of related WN4 and WN3 structures (e.g., Lin et al., 2007; H. Liu & Watanabe, 2008; Ren et al., 2009), and investigated the underlying mechanisms in further depth (e.g., Chang et al., 2013; Cho & Shepherd, 2015; He et al., 2011; Lei et al., 2014; Maute et al., 2012; Mukhtarov & Pancheva, 2011; Oberheide et al., 2011; Onohara et al., 2018).

In this work, we present observational evidence of prominent WN4 coupling between the lower thermosphere near 105 km and the ionospheric F-region at heights near 420 and 590 km during May 27–June 5, 2020. Our results take advantage of ion number density (hereafter, ion density) measurements from the Ion Velocity Meter (IVM) instruments onboard the Scintillation Observations and Response of The Ionosphere to Electrodynamics (SORTIE) and Ionospheric Connection Explorer (ICON) spacecraft and kinetic temperature observations from the Sounding of the Atmosphere using Broadband Emission Radiometry (SABER) instrument onboard the Thermosphere Ionosphere Mesosphere Energetics Dynamics (TIMED) satellite. We further connect this WN4 longitude variability to DE3 by spectrally analyzing ICON and SORTIE IVM data and investigate its latitude-height amplitude and phase structure using a Specified-Dynamics Whole Atmosphere Community Climate Model with thermosphere and ionosphere eXtension (SD/WACCM-X) simulation with realistic wave forcing imposed by nudging Modern-Era Retrospective analysis for Research and Applications version-2 (MERRA-2) reanalysis data in the troposphere and stratosphere. After a brief description of the data, models, and methods (Section 2), we present in detail the observational and modeling results regarding the WN4 variability and its connection to the DE3 tide (Section 3), and conclude with a brief summary (Section 4).

2. Data, Models, and Methods

2.1. SORTIE/IVM

SORTIE is a NASA Heliophysics System Observatory (HSO) 6U CubeSat mission to investigate the underlying causes behind the appearance of plasma structures in the F-region ionosphere, leading to equatorial plasma bubbles, and the evolution of these structures after their formation (Crowley et al., 2016). SORTIE was launched onboard Dragon CRS-19 to the International Space Station, from where it was deployed on February 19, 2020 in a nearly circular orbit near 420 km with $\sim 51.6^\circ$ inclination. It carries two science instruments, a miniature IVM, and a micro-Planar Langmuir Probe (Crowley et al., 2016). This study employs SORTIE's IVM Level 2 ion density data product with a 4-s temporal cadence.

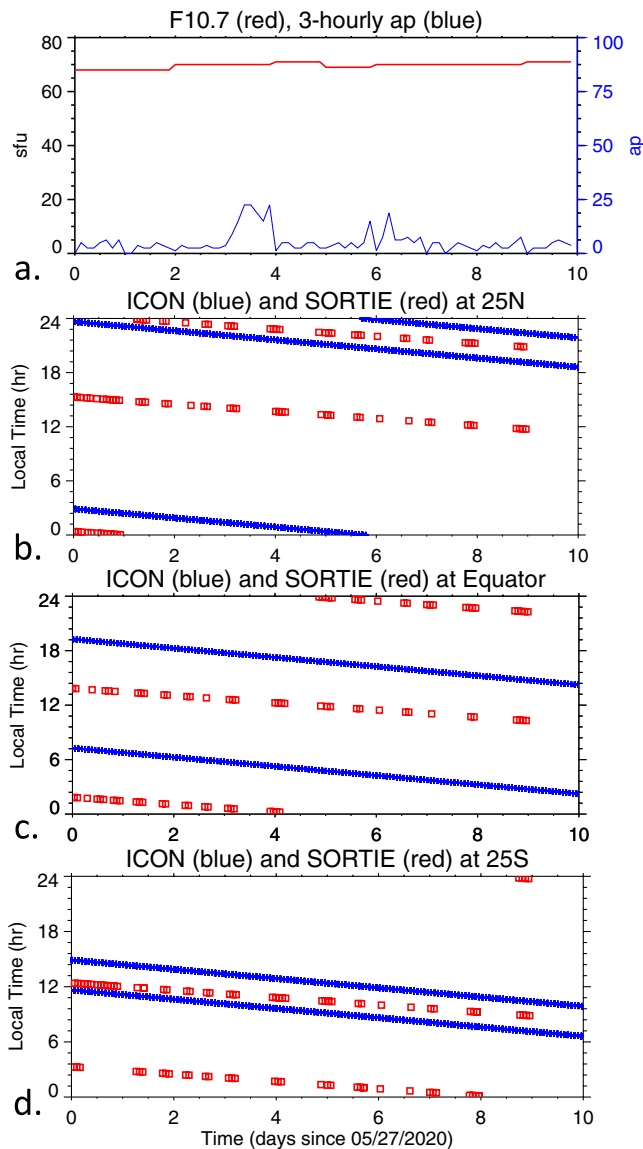


Figure 1. (a) Time series of the daily F10.7 solar flux (red curve) and 3-hourly ap (blue curve) during May 27–June 5, 2020. (b–d) Time series of Ionospheric Connection Explorer (ICON) (blue plus signs) and Scintillation Observations and Response of The Ionosphere to Electrodynamics (SORTIE) (red squares) local solar time at 25°N (panel b), equator (panel c), and 25°S (panel d).

2.2. ICON/IVM

ICON is a NASA HSO mission designed to study the fundamental connections between the dynamics of the neutral atmosphere at altitudes between 100 and 300 km and the charged particle motions at low and middle latitudes from a nearly circular orbit at an altitude near 590 km with $\sim 27^\circ$ inclination (Immel et al., 2018). The ICON payload includes an IVM instrument that provides in situ measurements of the ion drift motions, density, temperature and major ion composition (Heelis et al., 2017). The IVM comprises of two instruments, the Retarding Potential Analyzer (RPA) and the Drift Meter. This study employs ICON's IVM-A Data Product 2.7 v4 determined from RPA measurements, with a 1-s temporal cadence. Preliminary validation work by the ICON IVM team reports accuracy around $\pm 10^3 \text{ cm}^{-3}$ for this data product (see the acknowledgments for further information).

2.3. TIMED/SABER

The SABER instrument was launched onboard the TIMED satellite (also a NASA HSO mission) on December 7, 2001. SABER provides measurements of kinetic temperature from ~ 20 km to ~ 120 km altitude (Mertens et al., 2001). SABER views the atmospheric limb from an orbit of ~ 625 km altitude and $\sim 73^\circ$ inclination, so that the latitude coverage on a given day extends from about 53° in one hemisphere to about 83° in the other. This viewing geometry alternates once every ~ 60 days. Errors in the retrieved temperatures in the 80–105 km region are estimated to be ± 1.5 –5 K (Garcia-Comas et al., 2008). This study takes advantage of the SABER Level 2a Data Product with a ~ 55 -s temporal cadence.

2.4. WACCM-X

WACCM-X (J. Liu et al., 2018) is a configuration of the National Center for Atmospheric Research Community Earth System Model (Hurrell et al., 2013) that extends the atmospheric component into the thermosphere, with a model top boundary between 500 and 700 km. The standard spatial resolution of WACCM-X is 1.9° by 2.5° in latitude and longitude, respectively, and 1/4 scale height vertically above the upper stratosphere. To simulate the lower and middle atmosphere, WACCM-X can be run with SD that constrains the troposphere and stratosphere dynamics using MERRA-2 reanalysis data (Gelaro et al., 2017). This study employs output from an extended SD/WACCM-X version v2.1 simulation that covers the May 27–June 5, 2020 period. The empirical ion convection patterns are specified using the Heelis et al. (1982) empirical model. The MERRA-2 forcing provides a realistic representation of the wave forcing in the lower and middle atmosphere making this simulation an ideal physics-based framework for interpreting atmosphere-ionosphere coupling by tides.

2.5. Analysis of Satellite Data

When combined, the ascending and descending nodes of SORTIE and ICON cover 24-h of LT in ~ 30 days (i.e., each node samples ~ 4 h of LT in about 10 days). Figure 1 shows the LT coverage of ICON (blue plus signs) and SORTIE (red squares) IVM measurements at 25°N (panel b), at the equator (panel c), and at 25°S (panel d) during May 27–June 5, 2020. At the equator, SORTIE's (ICON's) orbit precesses from ~ 2 LT/ ~ 14 LT (~ 7 LT/ ~ 19 LT) on May 27 to ~ 22 LT/ ~ 10 LT (~ 2 LT/ ~ 14 LT) on June 5 (Figure 1c). As shown in Figure 1a, this 10-day period is characterized by low solar activity (average F10.7 ~ 70) with two minor

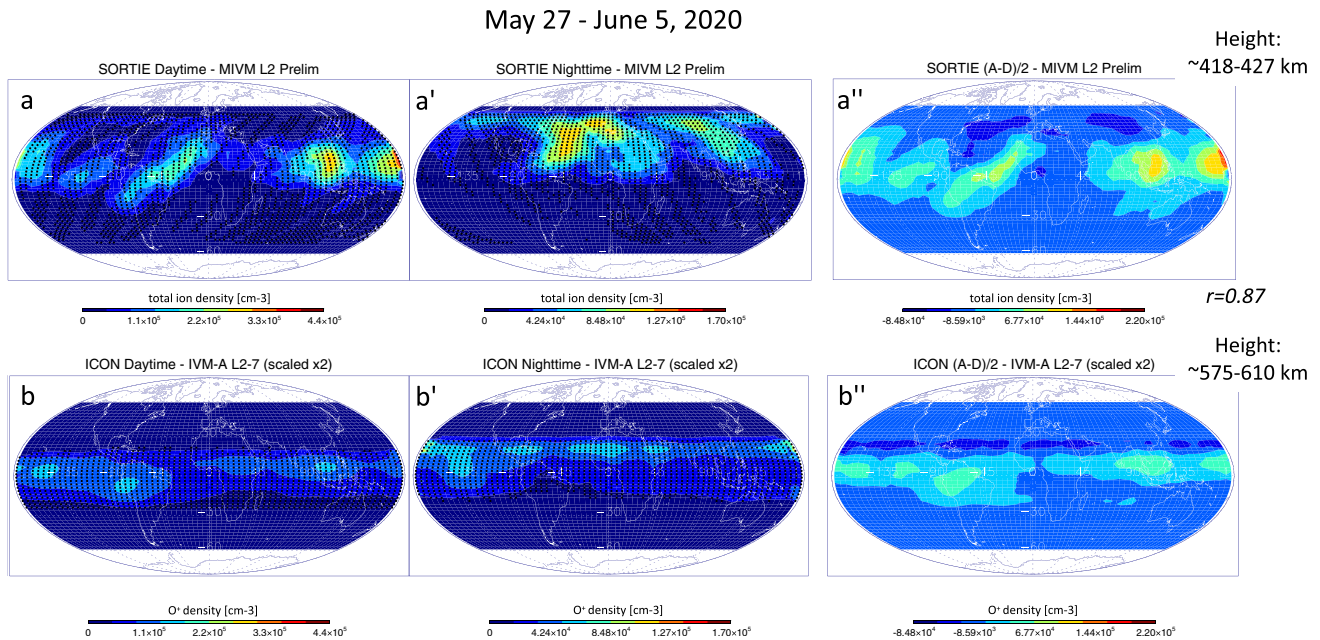


Figure 2. Latitude (60°S – 60°N) versus longitude (180°W – 180°E) maps of Scintillation Observations and Response of The Ionosphere to Electroynamics (SORTIE) total ion density (upper panels) and Ionospheric Connection Explorer (ICON) O^+ density (lower panels) Ion Velocity Meter (IVM) ion density measured during May 27–June 5, 2020. SORTIE (ICON) daytime, that is, ~ 10 – 14 local time (LT) (~ 14 – 18 LT), averages are shown in panel (a) (panel b); while SORTIE (ICON) nighttime, that is, ~ 22 – 2 LT (~ 2 – 6 LT) averages are shown in panel (a') (b'). Panels (a'' and b'') show maps of half ascending and descending node differences (i.e., daytime–nighttime differences). The black dots in panels (a–a') and (b–b') show the measurement locations. ICON O^+ ion density is scaled (multiplied) by a factor of 2 given ICON's higher mean altitude (~ 575 – 610 km) compared to SORTIE (~ 418 – 427 km). This scaling is performed to use the same color bar for both ICON and SORTIE. The correlation between the WN4 in SORTIE and ICON (panels a'' and b'') is $r = 0.87$ near the equator (10°S – 10°N), as noted at the bottom of panel (a''). MIVM, miniature IVM.

geomagnetic disturbances (ap ~ 25 on May 30, 2020 and ap ~ 15 on June 1–2, 2020). For this study, ICON and SORTIE IVM ion density are analyzed by both adding and subtracting ascending and descending node measurements. Wave analysis is performed by applying least squares methods to SORTIE IVM and ICON IVM ion density, and to SD/WACCM-X ion density and neutral temperature.

3. Results

The global distribution of ion density observed by SORTIE (ICON) IVM near 420 km (590 km) altitude during May 27–June 5, 2020 is presented in Figure 2. SORTIE daytime (~ 10 – 14 LT) and nighttime (~ 22 – 2 LT) 10-day averages are shown in panels a and b, respectively. Figures 2a' and 2b' show the corresponding ICON daytime (~ 14 – 18 LT) and nighttime (~ 2 – 6 LT) 10-day averages, respectively. Excellent low-latitude coverage is achieved by both SORTIE (about $\pm 51.6^{\circ}$ latitude) and ICON (about $\pm 27.1^{\circ}$ latitude) during this 10-day period, as evidenced by the distribution of the black dots in panels (a–a') and (b–b') showing the measurement locations. Ion density values up to $\sim 4.4 \times 10^5 \text{ cm}^{-3}$ ($\sim 2.1 \times 10^5 \text{ cm}^{-3}$) are observed during daytime and up to $\sim 1.7 \times 10^5 \text{ cm}^{-3}$ ($\sim 0.5 \times 10^5 \text{ cm}^{-3}$) during nighttime by SORTIE (ICON) IVM. Note that a scaling factor is applied multiplying the ICON ion density by a factor of 2 given ICON's higher mean altitude (i.e., ~ 590 km vs. ~ 420 km for SORTIE). Figures 2a''–2b'' display ascending and descending node differences for SORTIE and ICON IVM ion density, respectively, each scaled (multiplied) by 0.5. Both SORTIE and ICON show enhanced ion density at low latitudes around 30°S – 30°N with a prominent WN4 structure and peaks near 180°E , 100°E , 45°E , and 100°W . This type of feature in the low-latitude ionosphere was reported in previous satellite-based measurements (e.g., Immel et al., 2006; Lin et al., 2007; H. Liu & Watanabe, 2008; H. Liu et al., 2009), as discussed in Section 1. This notable WN4 structure observed by SORTIE and ICON points to a possible modulation of the background ion density by the nonmigrating DE3 tide as observed from their slowly precessing orbits. Note that while SORTIE IVM observes an O^+ -dominated ionosphere, ICON IVM samples nonnegligible H^+ (especially during nighttime). Thus, to best interpret the concurrent

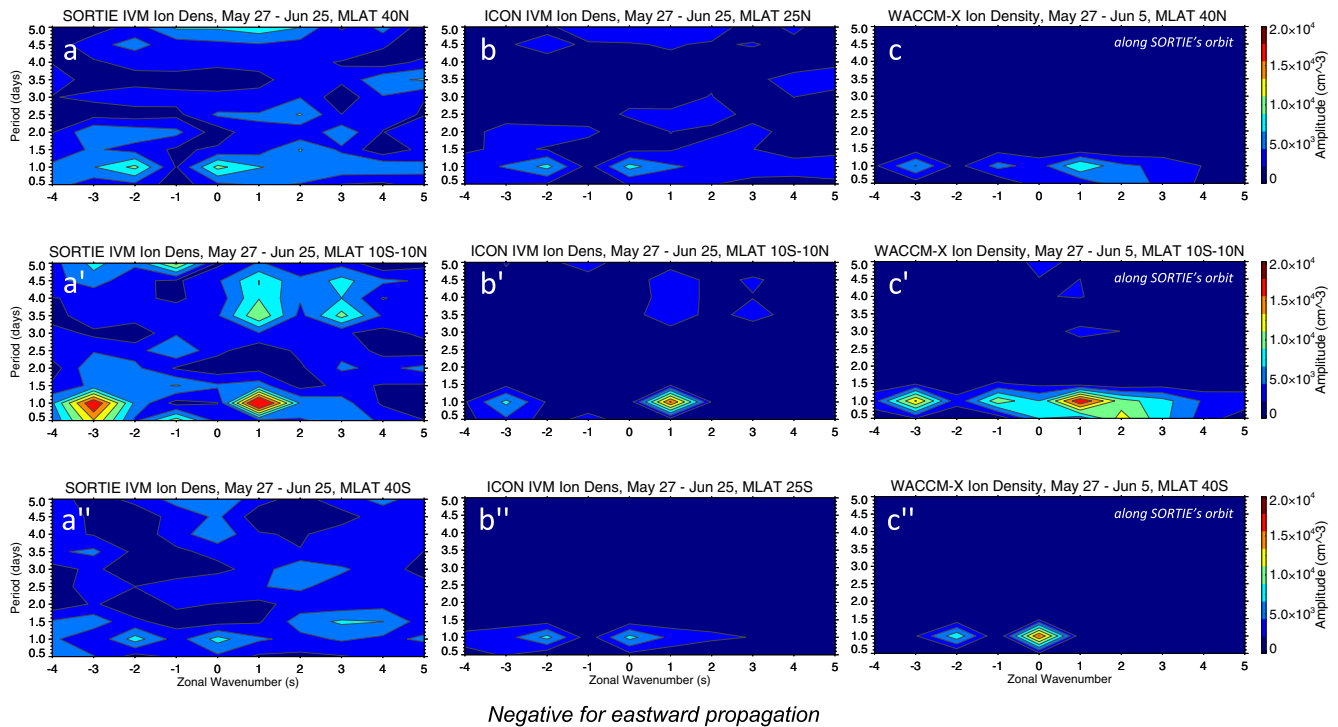


Figure 3. Period versus zonal wavenumber amplitude spectra of Scintillation Observations and Response of The Ionosphere to Electrodynamics (SORTIE) Ion Velocity Meter (IVM) ion density at magnetic latitude (MLAT) 40°N (panel a), 10°S–10°N (panel a'), and 40°S (panel a'') during May 27–June 25, 2020. (b–b'') Same as (a–a''), but for Ionospheric Connection Explorer (ICON) IVM O⁺ ion density at MLAT 25°N (panel b), 10°S–10°N (panel b'), and 25°S (panel a''). (c–c'') Same as (a–a''), but for Specified-Dynamics Whole Atmosphere Community Climate Model with thermosphere and ionosphere extension (SD/WACCM-X) ion density during May 27–June 5, 2020 and sampled along SORTIE's orbit. This 10-day window for WACCM-X is adopted for consistency with the SORTIE and ICON results shown in Figure 2. Eastward-propagating waves are indicated with negative wavenumbers. A prominent diurnal $s = -3$ diurnal eastward-propagating tide with zonal wavenumber 3 signal is clearly seen in the SORTIE, ICON, and SD/WACCM-X low-latitude ionosphere spectra, along with large DW1.

ionospheric WN4 signatures observed by ICON and SORTIE, Figures 2b–2b'' show ICON's O⁺ density. The Pearson correlation coefficient between the WN4 structure seen in the SORTIE total ion density and ICON O⁺ density (see Figures 2a''–2b'') is calculated to be ~ 0.87 . Also note that the equatorial ionization anomaly (EIA) is not evident in Figure 2 likely due SORTIE's and ICON's mean altitude (~ 420 km and ~ 590 km, respectively) being significantly higher than the F-layer peak height (~ 200 – 350 km), in agreement with Figure 2 of Mukhtarov and Pancheva (2011).

It is important to realize that while the variability due to the semidiurnal eastward-propagating tide with $s = -2$ (SE2) and stationary planetary wave 4 (SPW4) would largely be eliminated by the ascending/descending node differences shown in Figures 2a''–2b'' for latitudes less than about $\pm 10^\circ$ ($\pm 30^\circ$) for ICON IVM (SORTIE IVM), aliasing from the diurnal westward-propagating tide with $s = 5$ (DW5) and from the terdiurnal eastward-propagating tide with $s = -1$ (TE1) may also contribute to a WN4 longitude structure seen at a constant LT (see Gasperini et al., 2015, 2018, 2020; Gasperini, Hagan, & Zhao, 2017; Lieberman, 1991; Oberheide et al., 2000). Additionally, the LT difference between ICON's (SORTIE's) ascending and descending node IVM measurements is < 9 h for latitudes greater than around $\pm 10^\circ$ ($\pm 30^\circ$) (see Figure 1). Hence one can anticipate significant aliasing due to variability associated with SE2 and SPW4 at latitudes greater than around $\pm 10^\circ$ for ICON and $\pm 30^\circ$ for SORTIE due to this LT difference being < 9 h. Thus, to avoid these aliasing issues in the analysis of the WN4 structure, we (a) combine 30 days of SORTIE and ICON data collected during May 27–June 25, 2020 to acquire full 24-h LT coverage, and (b) use output from a 3-hourly SD/WACCM-X simulation. Figure 3 shows the period versus zonal wavenumber amplitude spectra of SORTIE IVM ion density and ICON IVM O⁺ ion density obtained by combining ascending and descending node measurements during May 27–June 25, 2020, and of SD/WACCM-X ion density during May 27–June 5, 2020 derived using the full model output. Around 10°S–10°N magnetic latitude (MLAT) SORTIE (panel a'),

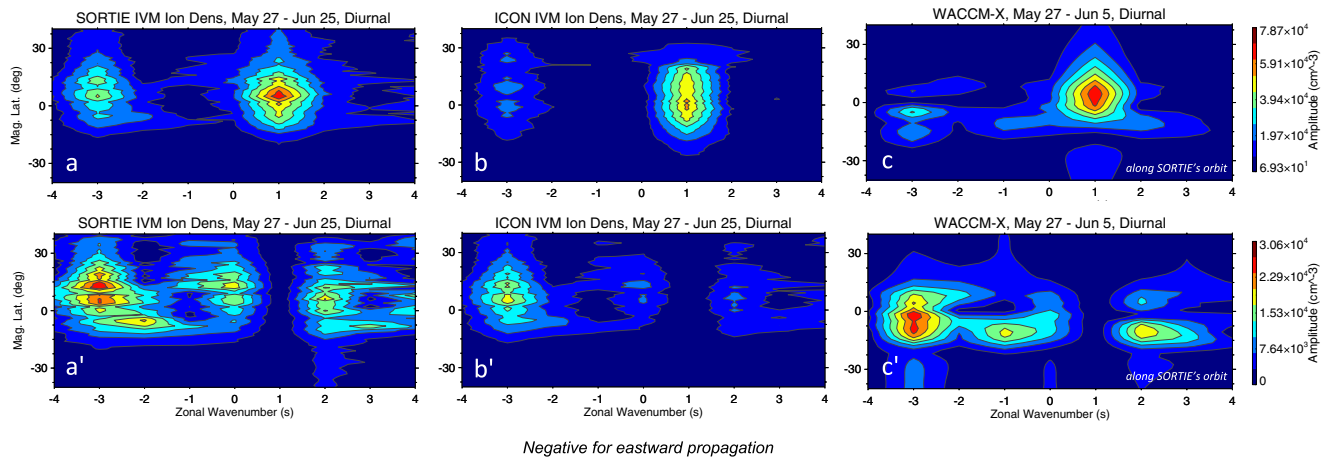


Figure 4. (a) Magnetic latitude (MLAT) versus zonal wavenumber diurnal amplitude spectra of Scintillation Observations and Response of The Ionosphere to Electrodynamics (SORTIE) Ion Velocity Meter (IVM) ion density during May 27–June 25, 2020. (b) Same as (a), but for Ionospheric Connection Explorer (ICON) IVM O^+ ion density. (c) Same as (a), but from Specified-Dynamics Whole Atmosphere Community Climate Model with thermosphere and ionosphere eXtension (SD/WACCM-X) output sampled along SORTIE's orbit during May 27–June 5, 2020. (a'–c') Same as (a–c), but with the migrating tide set to zero. The prominent ion density $s = -3$ diurnal eastward-propagating tide with zonal wavenumber 3 (DE3) variation exhibits amplitudes upward of $3 \times 10^4 \text{ cm}^{-3}$ in both the SORTIE observations (panel a') and the model (panel c'). ICON's DE3 ion density amplitude maxima are shown to be around $2.1 \times 10^4 \text{ cm}^{-3}$, that is, 30% lower than those found in SORTIE. The monthly averaged SORTIE and ICON diurnal ion density spectra are in general agreement, with similar latitudinal structures observed and predominant DW1, DE3, D0, and DE2 tidal signals.

ICON (panel b'), and WACCM-X (panel c') ion density spectra reveal the existence of a pronounced DE3 component with amplitudes up to $\sim 2 \times 10^4 \text{ cm}^{-3}$. DE3 is found to be nearly absent in both WACCM-X and the SORTIE (ICON) observations at 40°N MLAT (25°N MLAT) and 40°S MLAT (25°N MLAT), in agreement with the well-known Kelvin wave behavior of the first-symmetric equatorially trapped Hough mode of DE3 that efficiently propagates to the IT. The ion density DE3 observed by ICON is about 30% smaller than that observed by SORTIE. This amplitude difference between $\sim 420 \text{ km}$ and $\sim 590 \text{ km}$ is likely due to the combined influence of dissipation, zonal mean winds, wave-wave interactions, and inherent transience on the upward propagating thermospheric DE3. Also, present in the 10°S – 10°N MLAT spectra is the migrating DW1 tide, as shown in previous ionospheric observations (e.g., Chang et al., 2013). SW2, DW5, and TE1 amplitudes are found to be negligible (TE1 results not shown here), providing confidence to our assertion that the WN4 structure observed by SORTIE and ICON is in fact due to the nonmigrating DE3 tide.

To examine the latitudinal structure associated with this prominent F-region ion density DE3 (and other diurnal tides), Figure 4 shows the MLAT-wavenumber diurnal amplitude spectra of SORTIE IVM (panels a and a'), ICON IVM O^+ (panels b and b') and SD/WACCM-X (panels c and c') ion densities with and without the migrating DW1 tide set to zero. Similar to the results presented in Figure 3, SORTIE, ICON, and WACCM-X show general agreement with large DW1 ($\sim 7 \times 10^4 \text{ cm}^{-3}$) and DE3 (~ 2.1 – $3 \times 10^4 \text{ cm}^{-3}$) amplitude variations primarily confined to low latitudes. Along with pronounced DW1 and DE3 signals, the SORTIE and ICON spectra also exhibit D0 and DW2 variations (and some DE2 for SORTIE), while the WACCM-X spectra show DE1 and DW2 variations. Note that a $\sim 2 \times 10^4 \text{ cm}^{-3}$ DE2 amplitude variation is found in the model around 5°N – 20°N MLAT, but not in the SORTIE or ICON observations. Larger DE3 amplitudes (up to $3.06 \times 10^4 \text{ cm}^{-3}$) are found in the SORTIE and ICON spectra around 25°N – 10°S MLAT (panels 4a' and 4b', respectively) consistent with the results shown in Figures 3a' and 3b', while WACCM-X maxima are found near 10°N – 20°S MLAT. Some differences between the observed and modeled diurnal spectra are not unexpected and are likely due to (a) the different averaging window used (30 days for SORTIE and ICON, and 10 day for WACCM-X; note that a 10-day window for WACCM-X is adopted for consistency with the SORTIE and ICON results shown in Figure 2), (b) differences in the longitude-LT sampling between model and observations, and (c) inherent tidal variability observed by SORTIE and ICON that is not reproduced by the model. Even with the amplitude suppression associated with the monthly averaging, panel 4a' shows SORTIE IVM ion density DE3 amplitudes exceeding $\sim 3 \times 10^4 \text{ cm}^{-3}$, that is, over 15% of the observed zonal mean. As noted above in the context of Figure 3, the ICON observed ion density DE3 amplitudes are about

30% smaller than SORTIE. Although not addressed in this study, the noted amplitude difference may be ascribable to reduced thermospheric DE3 amplitudes near 590 km due to the combined influence of dissipation, zonal mean winds, and wave-wave interactions that may result in reduced in situ generated ion density DE3 at ICON heights. Follow on work will investigate these possible contributions to the observed amplitude differences (and day-to-day variability) using concurrent thermospheric observations by ICON. On the other hand, it is important to point out the remarkable degree of consistency between the SORTIE and ICON diurnal ion density spectra between ~ 420 km and ~ 590 km during May 27–June 25, 2020. The latitude structure of DW1, DE3, D0, and DE2 are similarly captured by both space-borne observational platforms. It will be interesting to investigate in detail the diurnal, semidiurnal, and terdiurnal tidal coupling between these two ionospheric regions and possible sources of latitude and temporal variability in the various tidal components. A few likely candidates responsible for the observed variability with height in the tidal amplitudes and latitude structures are noted above. A more systematic study that employs the entire ~ 5 -month period of simultaneous SORTIE and ICON observations and leverages other ICON remotely sensed thermospheric observations is currently underway.

Additional analysis of the DE3 tide in the ionosphere is performed using a 30-day sliding window of low-MLAT ($\pm 20^\circ$) SORTIE and ICON IVM ion density during the 4-month interval from May 27, 2020 through September 15, 2020 to investigate its temporal variability. Figure 5 shows daily variations of the estimated DE3 amplitudes (panel a) and phases (panel a') derived using a least squares method and the combined ascending/descending node data (i.e., covering ~ 24 -h LT). Both SORTIE and ICON DE3 amplitudes are found to be larger ($\sim 1.9 \times 10^4 \text{ cm}^{-3}$ for SORTIE and $\sim 1 \times 10^4 \text{ cm}^{-3}$ for ICON) around May 27–June 25, quickly decreasing to minima (10^3 – 10^4 cm^{-3} for SORTIE and ~ 800 – $2 \times 10^3 \text{ cm}^{-3}$ for ICON) near June–July, with largest amplitudes ($\sim 2.1 \times 10^4 \text{ cm}^{-3}$ for SORTIE and $\sim 1.3 \times 10^4 \text{ cm}^{-3}$) observed during mid-August through early September 2020. General agreement is found in the seasonal variation of the ion density DE3 amplitudes observed by SORTIE near 420 km and by ICON near 590 km, with some differences likely associated to additional complexities introduced by the influences of dissipation, zonal mean winds, and wave-wave interactions. The latitude structure of DE3 presented in Figure 4 and its temporal variation shown in Figure 5a, with largest amplitudes occurring around August–September and a second period of enhanced activity around April–May, is consistent with previous modeling work and observations (e.g., Gasperini et al., 2015; Mukhtarov & Pancheva, 2011; Truskowski et al., 2014). To investigate the altitude-latitude structure of the DE3 tide in the IT region, Figure 5b shows the SD/WACCM-X height (~ 100 – 450 km)–MLAT (60°S – 60°N) structure of ion density (panels b and b') and temperature (panels c and c') amplitudes and phases during May 27–June 5, 2020. Ionospheric DE3 amplitudes are found to be largest around the F-layer peak near 200–350 km, with a defined 2-peak structure and maxima of $\sim 8 \times 10^4 \text{ cm}^{-3}$ around 15°N and 15°S associated with the EIA (Appleton, 1946; Balan & Bailey, 1995). Previous studies (e.g., Immel et al., 2006; Sagawa et al., 2005; Wan et al., 2008) showed the EIA to exhibit a WN4 longitudinal variation and it is now well accepted that this structure in the ionospheric F-region can form as a result of the combined effect of the E-region dynamo modulation by the lower thermospheric DE3 and from the direct propagation of DE3 into the F-region. It is fairly well established that neutral density variations, changes in thermospheric atomic oxygen to nitrogen ratio, and meridional winds at F-region altitudes (e.g., England et al., 2010; H. Liu et al., 2009; Maute et al., 2012) can contribute to the coupling between the tides and the ionospheric plasma. Previous modeling and observational results (e.g., Oberheide et al., 2011) indicate small amplitudes (< 1 m/s) meridional DE3 winds in the low latitude (± 15 – 20°) middle and upper thermosphere, which suggests the thermospheric DE3 winds to be a minor contributor the observed ionospheric DE3 signature. Similarly, neutral density and thermospheric atomic oxygen to nitrogen ratio DE3 amplitudes are generally small at SORTIE and ICON altitudes. It would be beyond the scope of this study to investigate the relative contribution of these effects to the ionospheric DE3 observed by SORTIE and ICON and this effort is left for follow on work. The lower thermospheric temperature DE3 exhibits largest amplitudes of ~ 12 K around 110–120 km, in accord with previous modeling (e.g., Gasperini et al., 2015; Gasperini, Forbes, & Hagan, 2017) and observational (e.g., Truskowski et al., 2014) results. The vertical wavelength of the modeled temperature DE3 inferred from its vertical phase progression (panel c') is ~ 49.8 km, in line with a predominant first-symmetric Hough mode. Latitudinal asymmetries and broadening of the latitude structure with height in the thermospheric DE3 are likely due to the combined effect of mean winds and dissipation (e.g., Forbes, 2000; Gasperini et al., 2015; Gasperini, Forbes, & Hagan, 2017).

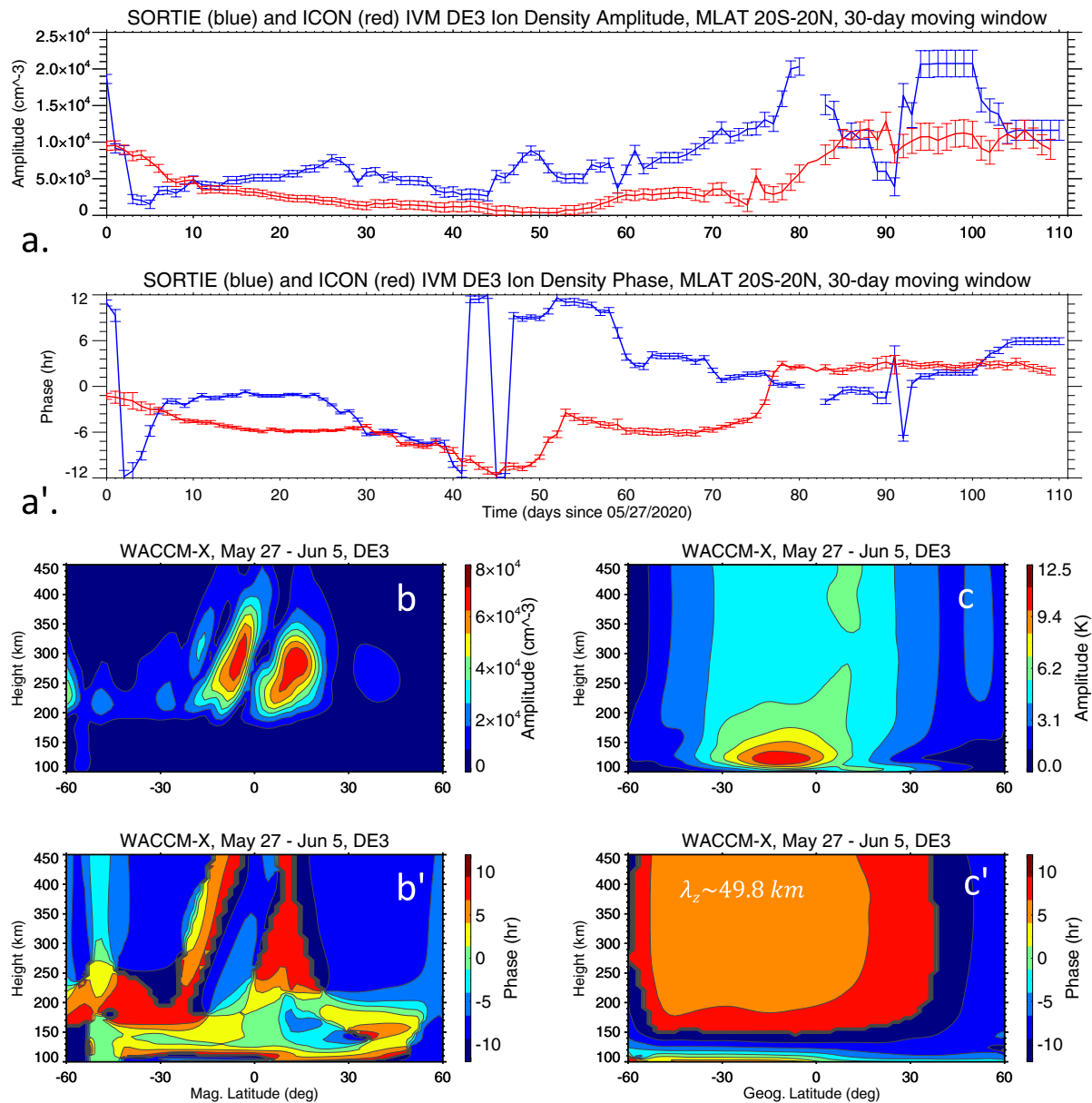


Figure 5. Time series of Scintillation Observations and Response of The Ionosphere to Electrodynamics (SORTIE) (blue line) and Ionospheric Connection Explorer (ICON) (red line) Ion Velocity Meter (IVM) ion density diurnal eastward-propagating tide with zonal wavenumber 3 (DE3) amplitudes (panel a) and phases (panel a') derived using least squares fitting within 30-day sliding windows during May 27–September 15, 2020. The vertical boxes identify 1- σ uncertainly estimates in the amplitudes and phases output by the fitting procedure. Panels (b–b') show the Specified-Dynamics Whole Atmosphere Community Climate Model with thermosphere and ionosphere eXtension (SD/WACCM-X) height (~100–450 km) versus magnetic latitude (MLAT) (60°S–60°N) ion density DE3 amplitudes and phases, respectively. Panels (c–c') show the same results as in panels (b–b'), but for neutral temperature DE3. The vertical wavelength of the modeled temperature DE3 inferred from its vertical phase progression (panel c') is ~ 49.8 km, consistent with a predominant first symmetric Hough mode.

Figure 6 displays maps of TIMED/SABER temperatures near 105 km observed concurrently (i.e., May 27–June 5, 2020) with the SORTIE and ICON IVM ion density maps presented in Figure 2. Panels a and b show results for the descending (~ 3 –5 LT) and ascending (~ 15 –17 LT) nodes, respectively; while panel c contains results for half ascending/descending node differences. A prominent WN4 structure is found to dominate the low-latitude ($\pm 30^\circ$) lower thermosphere with observed amplitude maxima of ~ 30 K peaking near 135°E, 75°E, 45°W, 135°W. Pearson correlation coefficients between the equatorial longitudinal WN4 structure in TIMED/SABER temperatures and the WN4 structure in SORTIE (ICON) IVM ion density are calculated to be $r = 0.71$ ($r = 0.67$). The correlation is computed on half ascending/descending node differences com-

TIMED/SABER Temperature V2.0, May 27 – June 5, 2020

Height: 105 km

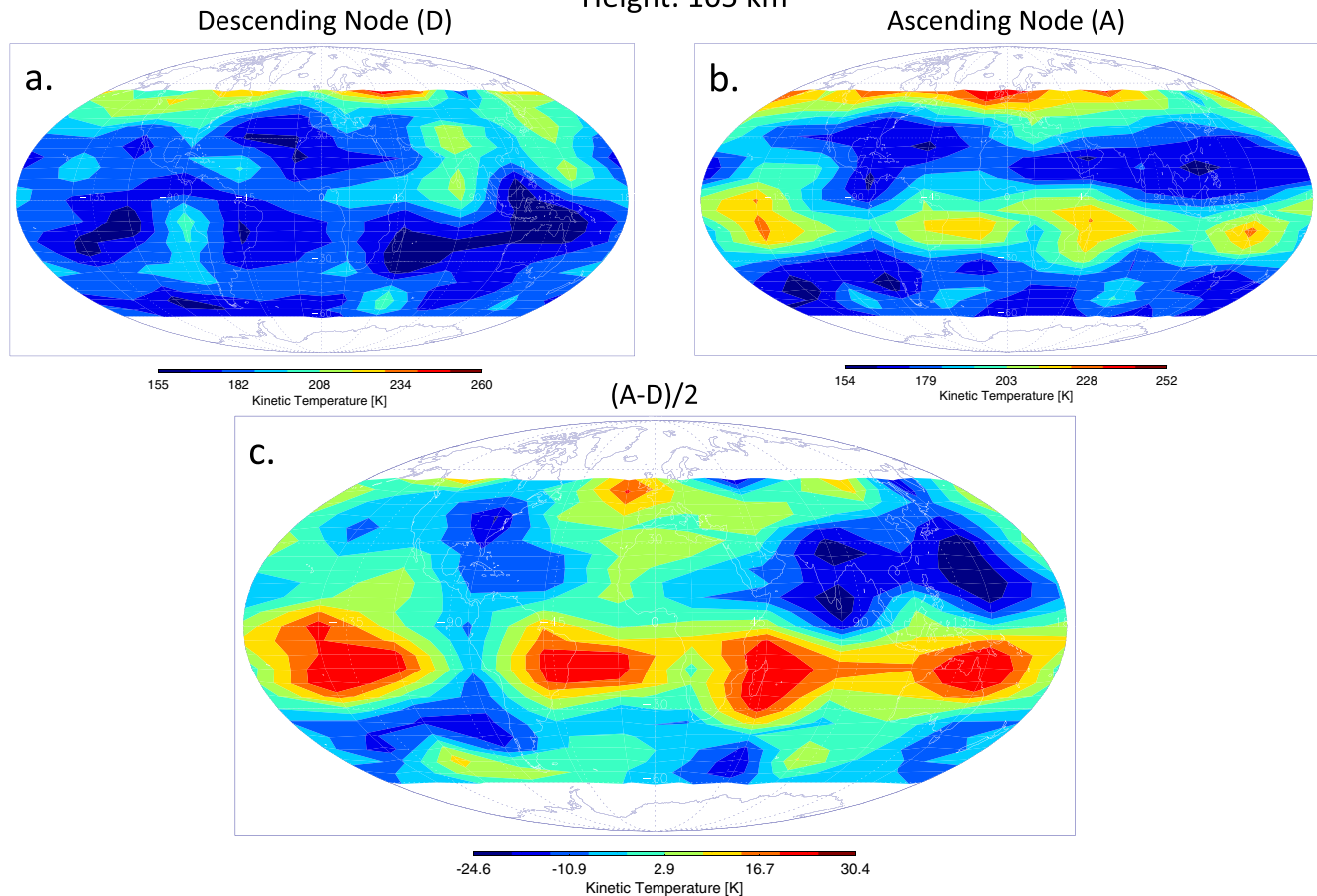


Figure 6. Latitude (60°S – 60°N) versus longitude (180°W – 180°E) maps of Thermosphere Ionosphere Mesosphere Energetics Sounding of the Atmosphere using Broad band Emission Radiometry (TIMED/SABER) kinetic temperatures near 105 km during May 27–June 5, 2020 at the descending node (panel a) near 3–5 local time (LT), ascending node (panel b) near 15–17 LT, and their half difference (panel c). A prominent longitudinal wavenumber-4 structure is evident in the differences (panel c) consistent with the concurrent ionospheric diurnal eastward-propagating tide with zonal wavenumber 3 signature observed by Scintillation Observations and Response of The Ionosphere to Electrodynamics (Ionospheric Connection Explorer) Ion Velocity Meter near 420 km (590 km).

binning data within 10°S – 10°N MLAT. This level of correlation, along with the modeling work discussed in Figure 5, provides strong evidence that the ionospheric WN4 structure observed by SORTIE and ICON is in fact associated with the lower thermospheric DE3. This level of correlation also indicates that there is significant phase coherence between the lower atmospheric DE3 and the F-region ion density DE3 near 420 and 590 km. This result agrees with our hypothesis that the F-region ion density DE3 is primarily driven by the E-region dynamo. As previously discussed, modeling and observational results generally demonstrate small meridional wind, neutral density, and atomic oxygen to nitrogen ratio DE3 amplitudes in the low-latitude (± 15 – 20°) middle and upper thermosphere. These considerations suggest that the in situ-driven component may be a minor component. An investigation on the relative contribution of the E-region dynamo modulation by the lower thermospheric DE3 versus the direct propagation of DE3 into the F-region is considered beyond the purview of the current investigation and will be the subject of a follow on work.

4. Summary and Conclusions

Results presented above provide a clear picture of a marked longitudinal WN4 variation observed during May 27–June 5, 2020 by SORTIE and ICON IVM in the low-latitude ionosphere near 420 and 590 km, respectively. Taking advantage of output from an SD/WACCM-X simulation nudged with MERRA-2 reanalysis data in the troposphere and stratosphere and monthly averaged SORTIE and ICON IVM data, this prominent WN4 structure in the F-region ion density is demonstrated to be due to the well-known DE3 tide. This nonmigrating tide has gained significant attention due to its ability to preferentially propagate to the IT from the tropical troposphere, thus effectively coupling these regions. SORTIE IVM (ICON IVM) observations and SD/WACCM-X output are shown to exhibit ion density DE3 amplitudes upward of $3 \times 10^4 \text{ cm}^{-3}$ ($2.1 \times 10^4 \text{ cm}^{-3}$), that is, over 15% of the zonal mean, around $\pm 20^\circ$ MLAT, with general agreement between model and observations. The monthly averaged SORTIE and ICON diurnal ion density spectra are found to be in strong agreement, with similar latitudinal structures observed and predominant DW1, DE3, D0, and DE2 tidal signals. DE3 ion density amplitudes are found to be about 30% smaller in ICON observations near 590 km compared to SORTIE observations near 420 km, possibly due to the combined effect of dissipation, mean winds, and wave-wave interactions on the thermospheric DE3 propagating between 420 and 590 km (e.g., Gasperini, Forbes, & Hagan, 2017).

Least squares fitting of monthly averaged SORTIE and ICON IVM ion density during May 27–September 15, 2020 showed larger ($\sim 1.9 \times 10^4 \text{ cm}^{-3}$ for SORTIE and $\sim 1 \times 10^4 \text{ cm}^{-3}$ for ICON) DE3 amplitudes around May 27–June 25, rapidly decreasing to smaller values (10^3 – 10^4 cm^{-3} for SORTIE and ~ 800 – $2 \times 10^3 \text{ cm}^{-3}$ for ICON) around June–July, and becoming largest ($\sim 2.1 \times 10^4 \text{ cm}^{-3}$ for SORTIE and $\sim 1.3 \times 10^4 \text{ cm}^{-3}$) around mid-August through early September 2020, in agreement with the well-known seasonal variation of DE3 amplitudes highlighted in previous modeling and observational studies (e.g., Gasperini et al., 2015; Gasperini, Forbes, & Hagan, 2017; Mukhtarov & Pancheva, 2011; Truskowski et al., 2014). Concurrent TIMED/SABER temperature observations near 105 km are shown to exhibit a pronounced WN4 structure (± 30 K) in the low-latitude lower thermosphere associated with DE3 that is found to be correlated with the ionospheric WN4 ($r = 0.71$ for SABER/SORTIE and $r = 0.67$ for SABER/ICON around 10°N – 10°S MLAT). Strong correlation ($r = 0.87$) is found between the WN4 structure observed simultaneously by SORTIE and ICON IVM. This level of correlation and the similarities in the SORTIE and ICON ion density DE3 latitude structures demonstrate that this tidal component is effective at coupling these two different ionospheric regions near 420 and 590 km simultaneously. Note that this period is generally characterized by small thermospheric DE3 amplitudes (e.g., Forbes et al., 2014; Gasperini et al., 2015; Oberheide et al., 2011). The less than perfect agreement (i.e., $r = 1.0$) between the two heights is ascribable to additional complexities on the thermospheric DE3 introduced by wave dissipation, the presence of zonal mean winds, possible wave-wave interactions, and inherent transience.

The latitude-height structure of this prominent DE3 signal is further investigated using SD/WACCM-X. DE3 amplitudes were found to be largest around the F-layer peak near 200–350 km, with two well-defined enhancements near 15°N and 15°S MLAT associated with the EIA and maxima of $\sim 8 \times 10^4 \text{ cm}^{-3}$. The modeled DE3 temperature amplitudes are found to exhibit largest amplitudes around 110–120 km, in accord with previous modeling and observational results (e.g., Gasperini et al., 2015; Gasperini, Forbes, & Hagan, 2017; Truskowski et al., 2014). Departure from a purely equatorially symmetric latitude structure and broadening of latitude structures with height of the thermospheric DE3 is explained in terms of the combined effect of mean winds and dissipation. The vertical wavelength of the modeled temperature DE3 is found to be ~ 49.8 km indicative of a predominant first symmetric Hough mode.

This study presented first, results of a prominent F-region ion density WN4 structure driven by the nonmigrating DE3 tide observed concurrently by the SORTIE CubeSat and ICON. The results herein contained provide evidence for the extent to which DE3 is capable of affecting simultaneously the global structure of the F-region ion density near 420 and 590 km. This study further demonstrates the degree to which global-scale tidal activity related to the tropical troposphere can influence the IT system. This study also demonstrates SORTIE and ICON to be excellent observational platforms for studying the influence of terrestrial weather on IT variability at low latitudes. Complementary and concurrent measurements from SORTIE's and ICON's near identical IVM instruments at different altitudes are shown to be particularly valuable.

Future work will take advantage of comprehensive sets of SORTIE and ICON observations to investigate in further detail the coupling of different IT regions by global-scale waves.

Data Availability Statement

ICON IVM-A data products (Level 2.7, Version 4) are publicly available at <https://spdf.gsfc.nasa.gov/pub/data/icon/l2/>. Post-processed SORTIE IVM Level 2 ion density data can be accessed on Zenodo at <https://doi.org/10.5281/zenodo.4589362>. TIMED/SABER temperatures (version v2.0) can be freely accessed at <http://saber.gats-inc.com/data.php/>. WACCM-X history files can be accessed at the NCAR/CDG (<https://doi.org/10.26024/5b58-nc53>) and are archived on the NCAR/HAO Campaign Space. For further information on the ICON IVM data used, see: <https://spdf.gsfc.nasa.gov/pub/data/icon/documentation/>. The post-processed data used for Figures 1–6 are available at <https://doi.org/10.5281/zenodo.4746615>.

Acknowledgments

The SORTIE mission is supported from NASA HQ by grant 80NSSC18K0094 to Atmospheric & Space Technology Research Associates (ASTRA) LLC. ICON is supported by NASA's Explorers Program through contracts NNG-12FA45C and NNG12FA42I. ASTRA is grateful for support from U. C. Berkeley and the ICON mission via Subcontract No: 00008210.

References

- Appleton, E. V. (1946). Two anomalies in the ionosphere. *Nature*, *157*, 691. <https://doi.org/10.1038/157691a0>
- Balan, N., & Bailey, G. J. (1995). Equatorial plasma fountain and its effects: Possibility of an additional layer. *Journal of Geophysical Research*, *100*, 21421–21432. <https://doi.org/10.1029/95JA01555>
- Chang, L. C., Lin, C.-H., Liu, J.-Y., Balan, N., Yue, J., & Lin, J.-T. (2013). Seasonal and local time variation of ionospheric migrating tides in 2007–2011 FORMOSAT-3/COSMIC and TIE-GCM total electron content. *Journal of Geophysical Research: Space Physics*, *118*, 2545–2564. <https://doi.org/10.1002/jgra.50268>
- Chapman, S., & Lindzen, R. S. (1970). *Atmospheric tides*. Springer.
- Cho, Y.-M., & Shepherd, G. (2015). Resolving daily wave 4 nonmigrating tidal winds at equatorial and midlatitudes with WINDII: DE3 and SE2. *Journal of Geophysical Research: Space Physics*, *120*(10), 10053–10068. <https://doi.org/10.1002/2015JA021903>
- Crowley, G., Fish, C., Pilinski, M., Stromberg, E., Huang, C., Roddy, O., et al. (2016). *Scintillation Observations and response of The Ionosphere to Electrodynamics (SORTIE)*. Proceedings of the 30th Annual AIAA/USU SmallSat Conference, Paper: SSC16-VI-3.
- England, S. L., Immel, T. J., Huba, J. D., Hagan, M. E., Maute, A., & DeMajistre, R. (2010). Modeling of multiple effects of atmospheric tides on the ionosphere: An examination of possible coupling mechanisms responsible for the longitudinal structure of the equatorial ionosphere. *Journal of Geophysical Research*, *115*, A05308. <https://doi.org/10.1029/2009JA014894>
- Fang, T.-W., Kil, H., Millward, G., Richmond, A. D., Liu, J.-Y., & Oh, S.-J. (2009). Causal link of the wave-4 structures in plasma density and vertical plasma drift in the low-latitude ionosphere. *Journal of Geophysical Research*, *114*, A10315. <https://doi.org/10.1029/2009JA014460>
- Forbes, J. M. (2000). Wave coupling between the lower and upper atmosphere: Case study of an ultra-fast Kelvin wave. *Journal of Atmospheric and Terrestrial Physics*, *62*, 1603–1621. [https://doi.org/10.1016/S1364-6826\(00\)00115-2](https://doi.org/10.1016/S1364-6826(00)00115-2)
- Forbes, J. M., Zhang, X., & Bruinsma, S. L. (2014). New perspectives on thermosphere tides: 2. Penetration to the upper thermosphere. *Earth, Planets and Space*, *66*(1), 122. <https://doi.org/10.1186/1880-5981-66-122>
- García-Comas, M., López-Puertas, M., Marshall, B. T., Wintersteiner, P. P., Funke, B., Bermejo-Pantaleón, D., et al. (2008). Errors in SABER kinetic temperature caused by non-LTE model parameters. *Journal of Geophysical Research*, *113*, D24. <https://doi.org/10.1029/2008JD010105>
- Gasparini, F., Forbes, J. M., Doornbos, E. N., & Bruinsma, S. L. (2015). Wave coupling between the lower and middle thermosphere as viewed from TIMED and GOCE. *Journal of Geophysical Research: Space Physics*, *120*, 5788–5804. <https://doi.org/10.1002/2015JA021300>
- Gasparini, F., Forbes, J. M., Doornbos, E. N., & Bruinsma, S. L. (2018). Kelvin wave coupling from TIMED and GOCE: Inter/intra-annual variability and solar activity effects. *Journal of Atmospheric and Solar-Terrestrial Physics*, *171*, 176–187. <https://doi.org/10.1016/j.jastp.2017.08.034>
- Gasparini, F., Forbes, J. M., & Hagan, M. E. (2017). Wave coupling from the lower to the middle thermosphere: Effects of mean winds and dissipation. *Journal of Geophysical Research: Space Physics*, *122*, 7781–7797. <https://doi.org/10.1002/2017JA024317>
- Gasparini, F., Hagan, M. E., & Zhao, Y. (2017). Evidence of tropospheric 90-day oscillations in the thermosphere. *Geophysical Research Letters*, *44*, 10125–10133. <https://doi.org/10.1002/2017GL075445>
- Gasparini, F., Liu, H., & McInerney, J. (2020). Preliminary evidence of Madden-Julian Oscillation effects on ultrafast tropical waves in the thermosphere. *Journal of Geophysical Research: Space Physics*, *125*, e2019JA027649. <https://doi.org/10.1029/2019JA027649>
- Gelaro, R., McCarty, W., Suarez, M. J., Todling, R., Molod, A., Takacs, L., et al. (2017). The modern-era retrospective analysis for research and applications, version 2 (MERRA-2). *Journal of Climate*, *30*, 5419–5454. <https://doi.org/10.1175/JCLI-D-16-0758.1>
- Hagan, M. E. (1996). Comparative effects of migrating solar sources on tidal signatures in the middle and upper atmosphere. *Journal of Geophysical Research*, *101*, 21213–21222. <https://doi.org/10.1029/96jd01374>
- Hagan, M. E., & Forbes, J. M. (2002). Migrating and nonmigrating diurnal tides in the middle and upper atmosphere excited by tropospheric latent heat release. *Journal of Geophysical Research*, *107*(D24), 4754. <https://doi.org/10.1029/2001JD001236>
- Hagan, M. E., Maute, A., Roble, R. G., Richmond, A. D., Immel, T. J., & England, S. L. (2007). Connections between deep tropical clouds and the Earth's ionosphere. *Geophysical Research Letters*, *34*, L20109. <https://doi.org/10.1029/2007GL030142>
- He, M., Liu, L., Wan, W., & Wei, Y. (2011). Strong evidence for couplings between the ionospheric wave-4 structure and atmospheric tides. *Geophysical Research Letters*, *38*, L14101. <https://doi.org/10.1029/2011GL047855>
- Heelis, R. A., Lowell, J. K., & Spiro, R. W. (1982). A model of the high-latitude ionospheric convection pattern. *Journal of Geophysical Research*, *87*, 6339–6345. <https://doi.org/10.1029/ja087ia08p06339>
- Heelis, R. A., Stoneback, R. A., Perdue, M. D., Depew, M. D., Morgan, W. A., Mankey, M. W., et al. (2017). Ion velocity measurements for the Ionospheric Connections Explorer. *Space Science Reviews*, *212*(1–2), 615–629. <https://doi.org/10.1007/s11214-017-0383-3>
- Hurrell, J. W., Holland, M. M., Gent, P. R., Ghan, S., Kay, J. E., Kushner, P. J., et al. (2013). The Community Earth System Model: A framework for collaborative research. *Bulletin of the American Meteorological Society*, *94*(9), 1339–1360. <https://doi.org/10.1175/BAMS-D-12-00121.1>

- Immel, T. J., England, S. L., Mende, S. B., Heelis, R. A., Englert, C. R., Edelman, J., et al. (2018). The Ionospheric Connection Explorer mission: Mission goals and design. *Space Science Reviews*, 214, 13. <https://doi.org/10.1007/s11214-017-0449-2>
- Immel, T. J., Sagawa, E., England, S. L., Henderson, S. B., Hagan, M. E., Mende, S. B., et al. (2006). The control of equatorial ionospheric morphology by atmospheric tides. *Geophysical Research Letters*, 33(15). <https://doi.org/10.1029/2006GL026161>
- Jin, H., Miyoshi, Y., Fujiwara, H., & Shinagawa, H. (2008). Electrodynamics of the formation of ionospheric wave number 4 longitudinal structure. *Journal of Geophysical Research*, 113, A09307. <https://doi.org/10.1029/2008JA013301>
- Lei, J., Thayer, J. P., Wang, W., Yue, J., & Dou, X. (2014). Nonmigrating tidal modulation of the equatorial thermosphere and ionosphere anomaly. *Journal of Geophysical Research: Space Physics*, 119, 3036–3043. <https://doi.org/10.1002/2013JA019749>
- Lieberman, R. S. (1991). Nonmigrating diurnal tides in the equatorial middle atmosphere. *Journal of the Atmospheric Sciences*, 48, 1112–1123. [https://doi.org/10.1175/1520-0469\(1991\)048<1112:ndtite>2.0.co;2](https://doi.org/10.1175/1520-0469(1991)048<1112:ndtite>2.0.co;2)
- Lieberman, R. S., Riggan, D. M., Ortland, D. A., Nesbitt, S. W., & Vincent, R. A. (2007). Variability of mesospheric diurnal tides and tropospheric diurnal heating during 1997–1998. *Journal of Geophysical Research*, 112, D20110. <https://doi.org/10.1029/2007JD008578>
- Lin, C. H., Hsiao, C. C., Liu, J. Y., & Liu, C. H. (2007). Longitudinal structure of the equatorial ionosphere: Time evolution of the four-peaked EIA structure. *Journal of Geophysical Research*, 112, A12305. <https://doi.org/10.1029/2007JA012455>
- Liu, H., & Watanabe, S. (2008). Seasonal variation of the longitudinal structure of the equatorial ionosphere: Does it reflect tidal influences from below? *Journal of Geophysical Research*, 113, A08315. <https://doi.org/10.1029/2008JA013027>
- Liu, H., Yamamoto, M., & Luhr, H. (2009). Wave-4 pattern of the equatorial mass density anomaly: A thermosphere signature of tropical deep convection. *Geophysical Research Letters*, 36, L18104. <https://doi.org/10.1029/2009GL039865>
- Liu, H.-L. (2016). Variability and predictability of the space environment as related to lower atmosphere forcing. *Space Weather*, 14, 634–658. <https://doi.org/10.1002/2016SW001450>
- Liu, J., Liu, H., Wang, W., Burns, A. G., Wu, Q., Gan, Q., et al. (2018). First results from the ionospheric extension of WACCM-X during the deep solar minimum year of 2008. *Journal of Geophysical Research: Space Physics*, 123, 1534–1553. <https://doi.org/10.1002/2017JA025010>
- Maute, A., Richmond, A. D., & Roble, R. G. (2012). Sources of low-latitude ionospheric E × B drifts and their variability. *Journal of Geophysical Research*, 117, A06312. <https://doi.org/10.1029/2011JA017502>
- Mertens, C. J., Mlynczak, M. G., López-Puertas, M., Wintersteiner, P. P., Picard, R. H., Winick, J. R., et al. (2001). Retrieval of mesospheric and lower thermospheric kinetic temperature from measurements of CO₂ 15 μm Earth limb emission under non-LTE conditions. *Geophysical Research Letters*, 28, 1391–1394. <https://doi.org/10.1029/2000gl012189>
- Mukhtarov, P., & Pancheva, D. (2011). Global ionospheric response to nonmigrating DE3 and DE2 tides forced from below. *Journal of Geophysical Research*, 116, A05323. <https://doi.org/10.1029/2010JA016099>
- Oberheide, J., Forbes, J., Hausler, K., Wu, Q., & Bruinsma, S. L. (2009). Tropospheric tides from 80–400 km: Propagation, inter-annual variability and solar cycle effects. *Journal of Geophysical Research*, 114. <https://doi.org/10.1029/2009JD012388>
- Oberheide, J., Forbes, J. M., Zhang, X., & Bruinsma, S. L. (2011). Wave-driven variability in the ionosphere-thermosphere-mesosphere system from TIMED observations: What contributes to the “wave 4”? *Journal of Geophysical Research*, 116, A01306. <https://doi.org/10.1029/2010JA015911>
- Oberheide, J., Hagan, M. E., Ward, W. E., Riese, M., & Offermann, D. (2000). Modeling the diurnal tide for the Cryogenic Infrared Spectrometers and Telescopes for the Atmosphere (CRISTA) 1 time period. *Journal of Geophysical Research*, 105(A11), 24917–24929. <https://doi.org/10.1029/2000JA000047>
- Onohara, A. N., Batista, I. S., & Batista, P. P. (2018). Wavenumber-4 structures observed in the low-latitude ionosphere during low and high solar activity periods using FORMOSAT/COSMIC observations. *Annals of Geophysics*, 36(2), 459–471. <https://doi.org/10.5194/angeo-36-459-2018>
- Ren, Z., Wan, W., Liu, L., & Xiong, J. (2009). Intra-annual variation of wave number 4 structure of vertical E B drifts in the equatorial ionosphere seen from ROCSAT-1. *Journal of Geophysical Research*, 114, A05308. <https://doi.org/10.1029/2009JA014060>
- Ren, Z., Wan, W., Xiong, J., & Liu, L. (2010). Simulated wave number 4 structure in equatorial F-region vertical plasma drifts. *Journal of Geophysical Research*, 115, A05301. <https://doi.org/10.1029/2009JA014746>
- Sagawa, E., Immel, T. J., Frey, H. U., & Mende, S. B. (2005). Longitudinal structure of the equatorial anomaly in the nighttime ionosphere observed by IMAGE/FUV. *Journal of Geophysical Research*, 110, A11302. <https://doi.org/10.1029/2004JA010848>
- Truskowski, A. O., Forbes, J. M., Zhang, X., & Palo, S. E. (2014). New perspectives on thermosphere tides—1. Lower thermosphere spectra and seasonal-latitude structures. *Earth, Planets and Space*, 66, 66–136. <https://doi.org/10.1186/s40623-014-0136-4>
- Wan, W., Liu, L., Pi, X., Zhang, M.-L., Ning, B., Xiong, J., & Ding, F. (2008). Wavenumber-4 patterns of the total electron content over the low latitude ionosphere. *Geophysical Research Letters*, 35, L12104. <https://doi.org/10.1029/2008GL033755>
- Wan, W., Ren, Z., Ding, F., Xiong, J., Liu, L., Ning, B., et al. (2012). A simulation study for the couplings between DE3 tide and longitudinal WN4 structure in the thermosphere and ionosphere. *Journal of Atmospheric and Solar-Terrestrial Physics*, 90–91, 52–60. <https://doi.org/10.1016/j.jastp.2012.04.011>
- Wan, W., Xiong, J., Ren, Z., Liu, L., Zhang, M.-L., Ding, F., et al. (2010). Correlation between the ionospheric WN4 signature and the upper atmospheric DE3 tide. *Journal of Geophysical Research*, 115, A11303. <https://doi.org/10.1029/2010JA015527>